Enhancing Performance of Convolutional Neural Network-based Epileptic Electroencephalogram Diagnosis by Asymmetric Stochastic Resonance

Zhuozheng Shi, Zhiqiang Liao, Hitoshi Tabata

***Abstract*— Epilepsy is a chronic disorder that leads to transient neurological dysfunction and is clinically diagnosed primarily by electroencephalography. Several intelligent systems have been proposed to automatically detect seizures, among which deep convolutional neural networks (CNNs) have shown better performance than traditional machine-learning algorithms. Owing to artifacts and noise, the raw electroencephalogram (EEG) must be preprocessed to improve the signal-to-noise ratio prior to being fed into the CNN classifier. However, because of the spectrum overlapping of uncontrollable noise with EEG, traditional filters cause information loss in EEG; thus, the potential of classifiers cannot be fully exploited. In this study, we propose a stochastic resonance-effect-based EEG preprocessing module composed of three asymmetrical overdamped bistable systems in parallel. By setting different asymmetries for the three parallel units, the inherent noise can be transferred to the different spectral components of the EEG through the asymmetric stochastic resonance effect. In this process, the proposed preprocessing module not only avoids the loss of information of EEG but also provides a CNN with high-quality EEG of diversified frequency information to enhance its performance. By combining the proposed preprocessing module with a residual neural network, we developed an intelligent diagnostic system for predicting seizure onset. The developed system achieved an average sensitivity of 98.96% on the CHB-MIT dataset and 95.45% on the Siena dataset, with a false prediction rate of 0.048/h and 0.033/h, respectively. In addition, a comparative analysis demonstrated the superiority of the developed diagnostic system with the proposed preprocessing module over other existing methods.**

The paper was submitted on December 2, 2022 for review. This work was supported in part by the Quantum Science and Technology Fellowship Program of the University of Tokyo; in part by the by the Basic Research Grant (Hybrid AI) of the Institute for AI and Beyond of the University of Tokyo; in part by the by the JST CREST under Grant JPMJCR22O2; and in part by the JSPS KAKENHI under Grant JP20H05651 and 23KJ0605. (Zhuozheng Shi and Zhiqiang Liao contributed equally to this work and should be regarded as co-first authors.) (Corresponding authors: Zhiqiang Liao; Hitoshi Tabata.)

Zhuozheng Shi and Hitoshi Tabata are with the Department of Bioengineering, Graduate School of Engineering, The University of Tokyo, 7-3-1 Hongo, Bunkyo-ku,Tokyo 113-8656, Japan (e-mail: shizhuozheng@g.ecc.u-tokyo.ac.jp; tabata@bioeng.t.u-tokyo.ac.jp).

Zhiqiang Liao and Hitoshi Tabata are with Department of Electrical Engineering and Information Systems, Graduate School of Engineering, The University of Tokyo, 7-3-1 Hongo, Bunkyo-ku, Tokyo 113-8656, Japan (e-mail: liao@bioxide.t.u-tokyo.ac.jp; tabata@bioeng.t.u-tokyo.ac.jp).

Index Terms— Asymmetric stochastic resonance, electroencephalography (EEG), epilepsy, seizure detection, deep learning.

I. INTRODUCTION

DUE to alterations in neuroglial cells, neurotransmitters, or ion channels, the neurons in the brains of epileptic patients frequently generate abnormal activities [1]. When seizures occur, there is potential for disturbances in a patient's awareness, movement, and other perceptual functions. Epilepsy patients experiencing irregular seizures in their daily life are at great risks, such as loss of control during driving vehicles and drowning during swimming. Although antiepileptic drugs can control the occurrence of some epileptic symptoms, they are not effective in approximately 30% of patients with epilepsy [2]. Therefore, it is essential to safeguard patients with epilepsy by monitoring and recognizing seizures. At present, the most commonly used clinical epilepsy diagnostic tool is multi-channel electroencephalogram (EEG), which records spontaneous, rhythmic electrical activity from brain cells. Although EEG has high temporal resolution, accurate diagnosis is time-consuming and difficult, even for highly trained neurologists [3]. To provide patients with high-quality EEG diagnosis and reduce the workload of clinicians, developing intelligent EEG diagnostic systems is of great significance and has been actively studied [4]–[7].

In the early stages of related research, epileptic EEG diagnosis required manual feature extraction and classification using traditional pattern recognition algorithms. For example, a seizure detection system proposed in 1982 used a simple classifier with extracted time-domain EEG features for automatic diagnosis [8]. The work in [9] introduced a multivariate technique that can extract spatial EEG features for a support vector machine (SVM) to realize seizure prediction. The method in [10] performed discrete wavelet transform (DWT) on the original EEG signal and extracted frequency features based on the covariance matrix in different band. The extracted features were then injected into the support vector machine (SVM) to identify epileptic activities. In [11], to extract the epileptic information contained in the chaotic behavior of the brain, entropy-based features were fused with the DWT-based and time-domain features. The most prominent features were then fed to a random forest (RF)

classifier to distinguish the cerebral state of epileptic patients. The good diagnostic accuracy demonstrated that these machine learning algorithms are effective tools for epileptic EEG interpretation and classification.

In contrast to traditional machine-learning algorithms that rely on high-quality handcrafted features, deep-learning methods that can automatically extract features have received wide attention in the past few decades. Among all deep-learning frameworks, convolutional neural networks (CNNs) are one of the most successful methods for biomedical applications [12]–[14]. In particular, there has been an emerging trend in the construction of CNN-based epileptic EEG diagnostic systems in recent years. Because CNNs can eliminate the feature extraction operation, the work in [15] directly inputs the raw EEG signals to the CNN for seizure detection. The hybrid CNN and long short-term memory (LSTM) network in [16] automatically predict seizures of patients with epilepsy based on DWT-processed EEG signals. In addition, some researchers have combined traditional feature extraction and CNNs to achieve better epilepsy diagnosis performance. For instance, the work [17] treats a common spatial pattern as a low-dimensional feature and inputs it into a shallow CNN for a seizure detection method having high-sensitivity. By combining the short-time Fourier transform and CNN, [18] used the two-dimensional features of EEG signals and successfully improved the seizure predictability. Hence, based on the abovementioned studies, it can be concluded that in terms of classification accuracy, the CNN-based algorithms outperform traditional feature extraction-based machine learning methods in epileptic EEG diagnosis. The good performance of CNNs can be attributed to its multi-convolution kernel and weight replication characteristics. The former enriches the EEG features automatically extracted by the CNN, whereas the latter reduces the complexity of the network and saves considerable computation time.

Irrespective of whether traditional machine learning or CNN-based methods are used for epileptic EEG diagnosis, preprocessing methods are required to remove the physiological artifacts and measurement noises that pollute EEG signals [19]. Commonly used filtering methods include traditional filters represented by band-pass filters [20], wavelet transform methods represented by the DWT [21], and empirical mode decomposition [22]. However, owing to the overlapping spectrum of noise and EEG, the above methods inevitably cause a loss of effective EEG information while removing noise components. It is generally believed that the loss of effective information negatively impacts the performance of a classifier [23].

Notably, weakly effective information can be amplified with the aid of noise perturbation in a specific nonlinear system [24]. In this process, noise is suppressed because of the energy transfer from the noise to information-carrying signals; thus, no effective information is lost. This counterintuitive phenomenon is referred to as the stochastic resonance (SR)effect, which has been widely studied in various weak signal amplification and noise reduction application scenarios, such as machine fault detection [25]–[27], visual perception [28] and binary classification [29], [30], and sensory enhancement of organisms [31], [32]. In the bioengineering field, the SR effect has also been used for MRI enhancement [33] and cardiac signal denoising [34], [35]. However, the nonlinear structure of these SR-benefited systems is limited to a single symmetric potential well, and to the best of our knowledge, there has been no relevant research on epileptic EEG processing.

Inspired by the fact that brain asymmetry is favorable for bioinformatic perception [36], we propose an asymmetric stochastic resonance unit (ASRU)-based preprocessing module for a CNN-based intelligent epilepsy EEG diagnostic system. In this study, a residual network with 50 layers (ResNet-50) was selected as the CNN classifier because of its versatility and excellent performance [37]. The ASRU preprocessing module consists of three parallel ASRUs, wherein the preprocessed output from each ASRU is independently connected to the input channel of ResNet-50. The degree of asymmetry of the three parallel ASRUs is different, which changes the escape rate between the asymmetric potentials. Consequently, in the process of using intrinsic noise energy to enhance EEG, the noise-induced gains of each EEG frequency component are different. This leads to an effect similar to the attention mechanism in transformers [38], which enables each input channel of the CNN to focus on the information of different frequency bands in the EEG. It is worth noting that the nonlinear structure of the ASRU is an overdamped bistable potential well that has been proven to provide short-term memory capacity. Therefore, applying the proposed ASRU module not only prevents effective information loss, but also enhances the learning ability of the CNN.

The remainder of this paper is organized as follows. In Section II, our intelligent epileptic EEG classification system is explained in detail, including the mechanism of the ASRU module, structure of ResNet-50, and adaptive parameter optimization strategy. In Section III, a performance comparison between the proposed ASRU module and baseline preprocessing methods with ResNet-50 is conducted on the CHB-MIT and Siena datasets. The CHB-MIT and Siena datasets contain multi-channel continuously recorded scalp EEG, which is more realistic and challenging. In addition, the experimental results of the comparison using different metric functions and classifiers are also presented in this section. In Section IV, the computational speed and hardware realization potential of the proposed method are discussed, followed by a comparison with existing methods. Section V presents conclusions and suggests future research directions.

II. METHODOLOGY

A. Deep learning-based epileptic EEG diagnosis process

A schematic of the deep learning-based epileptic EEG diagnosis process adopted in this study is shown in Fig. 1. First, the information flow of multi-channel EEG signals

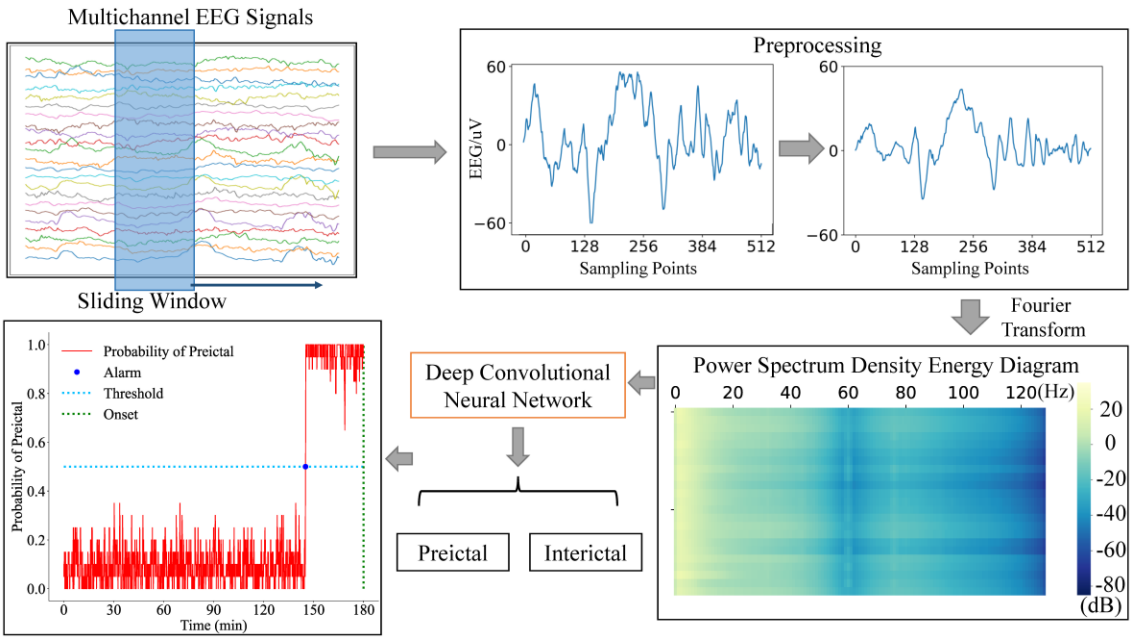

Fig. 1. Schematic of the overall deep CNN-based epileptic EEG classification and prediction process.

intercepted by the sliding window were preprocessed to remove interfering components, such as physiological artifacts and device noise [19]. After preprocessing, the time-domain EEG signals were converted into frequency-domain information as the input to the deep learning module. This is because previous studies have pointed out that the statistical changes in epileptic EEG in different periods are obvious in the frequency domain [39]–[41]. At this stage, the EEG of each channel was converted to a power spectrum density (PSD) that can characterize the energy distribution of the signal in the frequency domain. Thereafter, the EEG PSD of all channels were arranged together, and the PSD energy diagram (PSDED) could be obtained, as shown in the bottom right of Fig. 1. The subsequent deep CNN can learn features of EEG samples. For each EEG sample, the CNN model produces two probability values: the probability of the sample being classified as a preictal recording (P) and the probability of the sample being classified as an interictal recording ($1-P$). For eliminating fluctuations in P, referring to the previous research [41], a moving average method spanning 20 points is employed to smooth P. A seizure alarm is triggered when the smoothed P exceeds a threshold of 50%, as shown in the bottom left of Fig. 1.

B. Preprocessing by ASRU

1) Nonlinear structure of the ASRU

When a Brownian particle moves in an asymmetric overdamped bistable system under the influence of an external driving force $s(t)$ and a random noise $\xi(t)$, its dynamics can be described by the following simplified Langevin equation:

$$\frac{dx}{dt} = -U'(x) + s(t) + \xi(t), \tag{1}$$

where x is the trajectory of a Brownian particle. If $\xi(t)$ is assumed as Gaussian white noise with a noise intensity of D, it satisfies $\langle \xi(t)\xi(t_0)\rangle = 2D\delta(t-t_0)$. $U(x)$ is the asymmetric potential function, which can be written as:

$$U(x) = \begin{cases} -\frac{1}{2}ax^2 + \frac{1}{4}bx^4, & x \geq 0 \\ -\frac{1}{2}aAx^2 + \frac{1}{4}bBx^4, & x < 0 \end{cases}, \tag{2}$$

where a and b are the structural coefficients that control the shape of the potential wells, and A and B are asymmetry coefficients. By considering $U(x)' = 0$, the extreme value of $U(x)$ can be obtained as:

$$\begin{cases} x_+ = \sqrt{\frac{a}{b}} \\ x_0 = 0 \\ x_- = -\sqrt{\frac{aA}{bB}} \end{cases}. \tag{3}$$

where x_+ and x_- are stable extreme points, whereas x_0 is unstable. Assuming $A = B = k$, x_+ and x_- are origin-symmetric. In this case, as depicted in Fig. 2(a), adjusting k can change the depth of the left-half well of $U(x)$ without affecting the width. For simplicity, we refer to this as ASRU with regulating depth (ASRU-RD). If we assume $A = 1/k^2$ and $B = 1/k^4$, the depths $h_\pm$ of both the stable points satisfy $h_\pm = a/(4b^2)$. As depicted in Fig. 2(b), adjusting k in this case can change the width of the left-half well of $U(x)$ without affecting the depth. Similarly, we call this ASRU with regulating width (ASRU-RW). Whether the well depth or width is adjusted, $k = 1$ indicates that the ASRU degenerates into a symmetric stochastic resonance unit (SSRU).

2) Numerical solution of the ASRU

Generally, the analytical solution of x cannot be obtained using (1). Hence, the fourth-order Runge–Kutta method was adopted in this study to calculate the numerical solution of x. The calculation process is as follows.

$$k_1 = h(-U'(x(n)) + s(n)) + \sqrt{h}\xi(n), \tag{4}$$

$$k_2 = h(-U'\left(x(n) + \frac{k_1}{2}\right) + s(n)) + \sqrt{h}\xi(n)), \tag{5}$$

$$k_3 = h(-U'\left(x(n) + \frac{k_2}{2}\right) + s(n+1)) + \sqrt{h}\xi(n+1), \tag{6}$$

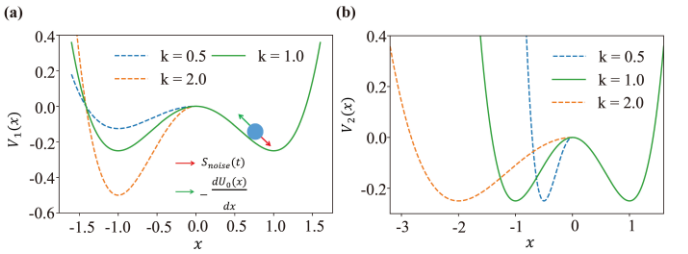

Fig. 2. (a) Potential function $U(x)$ with $a = b = 1$ and $A = B = k$. The depth of left potential well can be changed by adjusting k. (b) Potential function $U(x)$ with $a = b = 1$, $A = 1/k^2$, and $B = 1/k^4$. The width of left potential well can be changed by adjusting k.

$$k_4 = h(-U'(x(n) + k_3) + s(n+1)) + \sqrt{h}\xi(n+1), \quad (7)$$

$$x(n+1) = x(n) + \frac{1}{6}(k_1 + 2k_2 + 2k_3 + k_4), \quad (8)$$

where $x(n)$, $s(n)$, and $\xi(n)$ are the discrete expressions for $x(t)$, $s(t)$, and $\xi(t)$, respectively. h denotes the calculation step size, which affects the accuracy of the calculation. h was set to 0.1 in this study, in accordance with a previous study [35].

3) Denoising and output characteristic of ASRU

Assuming that the system described in (1) can reach local equilibrium in sufficient time, according to the approximate solution of the Fokker-Planck-Kolmogorov equation [42], the quasi-steady-state distribution function $\rho_{st}(x,t)$ can be expressed as:

$$\rho_{st}(x,t) = \frac{L}{F(x)} e^{\int \frac{E(x)}{F(x)} dx} = \frac{L}{\sqrt{F(x)}} e^{-\frac{\varphi(x,t)}{D}}, \quad (9)$$

where L is the normalization constant of the stochastic dynamics and $\varphi(x,t)$ represents the generalized potential. $E(x)$ and $F(x)$ are the drift term and diffusion term of the stochastic dynamics, respectively. The mathematical expressions of $E(x)$ and $F(x)$ are as follows:

$$E(x) = -U'(x) + s(t) + \frac{1}{2}F'(x), \quad (10)$$

$$F(x) = \frac{D}{1-\tau\mathbb{R}}, \quad (11)$$

with

$$\mathbb{R} = \begin{cases} -U''(x_+) & , x \in [0, +\infty] \\ -U''(x_-) & , otherwise \end{cases}, \quad (12)$$

where is the autocorrelation time of the noise term.

Considering the Kramers-like approximation, the mean first-passage time of Brownian particles hopping between two stable points can be written as follows [43]:

$$\begin{cases} T_{x_+ \to x_-} = \int_{x_-}^{x_+} \frac{dx}{F(x)\rho_{st}(x,t)} \int_{x}^{+\infty} \rho_{st}(y,t)dy \\ T_{x_- \to x_+} = \int_{x_-}^{x_+} \frac{dx}{F(x)\rho_{st}(x,t)} \int_{-\infty}^{x} \rho_{st}(y,t)dy \end{cases}. \quad (13)$$

The integral calculations in (13) are too complex to be calculated analytically. Hence, we used the steepest-descent approximation to simplify it as

$$\begin{cases} T_{x_+ \to x_-} \approx 2\pi |U''(x_+)U''(x_0)|^{-\frac{1}{2}} \exp\left[-\frac{\varphi(x_+,t) - \varphi(x_0,t)}{D}\right] \\ T_{x_- \to x_+} \approx 2\pi |U''(x_-)U''(x_0)|^{-\frac{1}{2}} \exp\left[-\frac{\varphi(x_-,t) - \varphi(x_0,t)}{D}\right] \end{cases}. \quad (14)$$

The probabilities $p_\pm(t)$ of the Brownian particles on either side of the potential well satisfy the following formula:

$$p_+(t) + p_-(t) = 1. \quad (15)$$

Thus, the evolution of $p_+(t)$ can be described by the following master equation:

$$\begin{aligned} \dot{p_+}(t) &= -\dot{p}_-(t) \\ &= \frac{p_-(t)}{T_{x_- \to x_+}} - \frac{p_+(t)}{T_{x_+ \to x_-}} \\ &= \frac{1 - p_+(t)}{T_{x_- \to x_+}} - \frac{p_+(t)}{T_{x_+ \to x_-}}. \end{aligned} \quad (16)$$

For simplification, we first consider a situation in which the noise is zero-mean Gaussian white noise, and the input is a sinusoidal signal with an amplitude of 0.35. Assuming $a = b = k = 1$, $U(x)$ becomes a symmetric bistable potential with a transition threshold of 0.385 [44]. For such a bistable system, the output signal-to-noise ratio (SNR) can be obtained by integrating (16) and calculating the autocorrelation function. Combined with (14), one can know that the output SNR satisfies the following relationship:

$$SNR \propto \frac{1}{D^2} \exp\left[-\frac{h_\pm}{D}\right]. \quad (17)$$

Equation (17) shows that the output SNR of the ASRU first increased and then decreased with an increase in D. As illustrated in Fig. 3(a), when D=0, the output of the SSRU can vibrate only on one side of the potential well, and the amplitude was reduced. When the noise intensity was appropriate (D=1.2), the sinusoidal signal submerged by the noise was amplified and accompanied by a significant weakening of the noise, as shown in Fig. 3(b). If the noise intensity in the SSRU is excessive, the effective information of the sinusoidal signal cannot be extracted from the noise, as shown in Fig. 3(c). As can be observed in Figs. 3(d)–(i), the cases of ASRU are similar to those of SSRU. The intuitive difference between them is that, when the well depth is adjusted, the output signal should have a greater amplitude on the side of the deeper potential well, as depicted in Fig. 3(e). Likewise, when the well width is adjusted, the signal should stay for more time in the wider potential well, as depicted in Fig. 3(h).

Subsequently, we assumed a complex signal containing multiple frequency components as the input signal of the

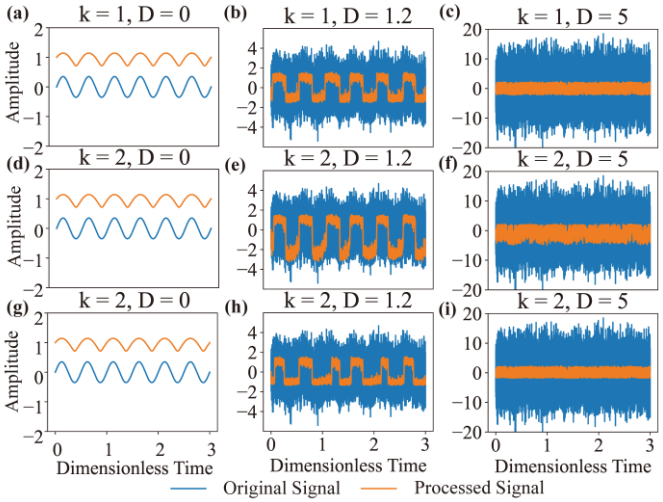

Fig. 3. The original input signal and the processed signal by an SSRU when (a) $D = 0$, (b) $D = 1.2$, and (c) $D = 5$. The original input signal and the processed signal by an ASRU-RD when (d) $k = 2, D = 0$, (e) $k = 2, D = 1.2$, and (f) $k = 2, D = 5$. The original input signal and the processed signal by an ASRU-RW when (g) $k = 2, D = 0$, (h) $k = 2, D = 1.2$, and (i) $k = 2, D = 5$. The structure coefficients are normalized.

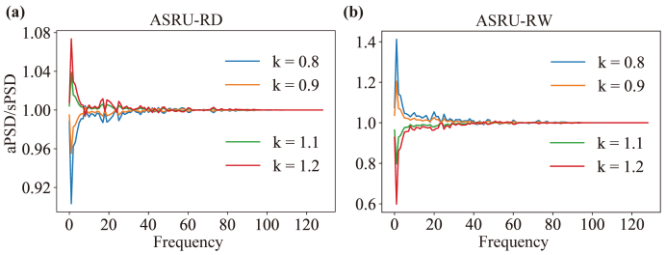

Fig. 4. (a) Ratio of PSD output by ASRU-RD at different k to PSD output by SSRU. (b) Ratio of PSD output by ASRU-RW at different k to PSD output by SSRU. The structure coefficients are normalized.

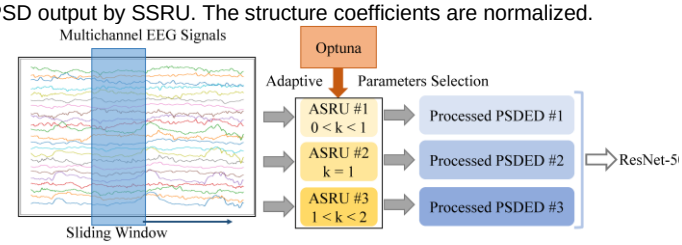

Fig. 5. Schematic of the ASRU preprocessing module.

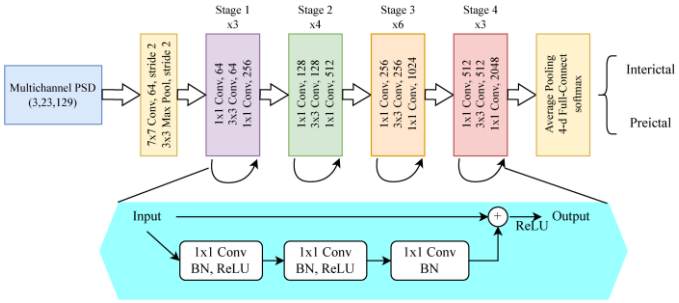

Fig. 6. Schematic of ResNet-50. The structure of the residual block with identity shortcut connection is shown in the blue block below.

TABLE I
Floating point operations (FLOPs) of the ResNet with different layer numbers

Layer number	ResNet-18	ResNet-34	ResNet-50	ResNet-101	ResNet-152
FLOPs	1.8×10^9	3.6×10^9	3.8×10^9	7.6×10^9	11.3×10^9

ASRU. If the left well was deeper, the left side of the potential barrier was steeper, which increases the damping term $-U'(x)$ near the barrier. Accordingly, there is an increase in the $T_{x_-\to x_+}$ required for Brownian particles to transition from the left to the right well. For the high-frequency component of the input signal, a large $T_{x_-\to x_+}$ is not conducive to its escape from the left potential well. In contrast, in this case, it is conducive to the transition between the two potential wells for the low-frequency component of the signal. Hence, one can conclude that the increase in k in the ASRU-RD makes it easier to enhance low-frequency information, and vice versa. Taking the EEG signal as an example, Fig. 4(a) shows the ratio of the PSD output by the ASRU-RD (denoted as "aPSD") at different k to PSD output by SSRU (denoted as "sPSD"). Consistent with the previous analysis, when the left potential well was deeper, the low-frequency energy was larger than the high-frequency energy of the processed EEG signal. In contrast, when the left potential well became shallow, the low-frequency component of the ASRU-processed signal was more suppressed than the high-frequency component. Similar to the case of the ASRU-RD, narrowing the well width makes the left side of the potential barrier steeper. This implies that $T_{x_-\to x_+}$ is increased, which has the an effect similar to increasing the well depth. Hence, as displayed in Fig. 4(b), one can show that the decrease in k in ASRU-RW makes it easier to enhance the low-frequency information of the EEG signal, and vice versa.

5) Structure of ASRU preprocessing model

In the image processing field, where CNNs originate, visual images are usually decomposed into RGB data. This operation can utilize the multi-channel advantages of the CNN and help the CNN extract image features from different dimensions. Using this as the inspiration, the structure of the ASRU module for EEG preprocessing was set to take full advantage of the multi-channel advantages of the CNN, as shown in Fig. 5. Firstly, the raw EEG recording intercepted by the sliding window of each channel was input into three parallel ASRU units. Then, for each ASRU, the processed EEG recordings of all channels were combined and Fourier transformed to obtain a PSDED graph, which was used as input for the CNN. Notably, the asymmetry type (regulating depth and width) and structure coefficients (a, b) of the three parallel ASRUs were concordant. This can reduce the computation cost in parameter optimization and ensure that the asymmetry of the three parallel ASRUs is different. Using this setup, the energy of the corresponding frequency components is different for the output EEG signals from the three parallel ASRUs.

From the analysis of Fig. 3 and related studies [33–35], it is clear that there is an optimal noise intensity that optimizes the performance of the SR system. Generally, if the noise intensity in the signal is known, the parameters a and b can be adjusted to change the shape of the SNR curve of the SR system [44]. By matching the optimal noise intensity required by the system and the noise intensity in the input signals, the noise energy can be maximally transferred to the effective information. However, since the noise intensity in the recorded biological signals is uncontrollable, it is difficult to manually adjust parameters without prior knowledge of noise.

To automatically select the optimal parameters of ASRU for epileptic EEG classification, the Optuna optimization algorithm was adopted in this study. Optuna is an open-access heuristic optimization algorithm [45], which is suitable for users without the relevant technical background to utilize. When using Optuna to optimize the ASRU, several points should be noted regarding Optuna. First, the search space of Optuna is dynamically constructed, which means that users do not need to participate in designing internal variables. Second, Optuna performs sampling during optimization, including relational sampling using multi-parameter correlation and independent sampling with individually evaluated parameters. These two sampling strategies make Optuna suitable for optimizing systems with highly correlated hyperparameters. Third, the setup of Optuna only involves importing packages, defining the objective function, and specifying the hyperparameters to be optimized. In this work, the sensitivity of the entire system to predict seizure was set as the objective function.

C. ResNet-based CNN classifier

According to the universal approximation theorem, given a

sufficient capacity, a single-layer feed-forward network is sufficient to approximate any function. This may require the network to be sufficiently large, leading to overfitting. Therefore, researchers have developed deeper network architectures. However, due to the gradient vanishing, the training and testing errors of a multilayer plain CNN network without a shortcut connection increase as the network deepens [37]. To solve this problem, some researchers introduced the structure of an identity shortcut connection into the traditional deep neural networks. Because the gradient information of the former layer is retained in that of the deeper layer through identity shortcut connection, we only need to ensure that the gradient of the shallow layer is not too small to avoid gradient vanishing. Deep neural networks with this structure are also known as ResNet, which can improve its performance by increasing the number of hidden layers [37].

In this study, the most widely used CNN-based ResNet was adopted. As shown in Table I, the computational complexity increased with the number of layers. Considering the computational performance and overhead, we chose ResNet-50 as the deep-learning module for the epileptic EEG classification system. The specific network topology of ResNet-50 is shown in Fig. 6.

D. Cross-validation-based training and testing

In order to reduce the randomness in performance evaluation, the proposed epileptic EEG diagnosis model requires a testing and training scheme based on the subject-specific leave-one-out cross validation to establish a testing and training scheme [41], [46]. Assuming a patient experiences L seizures, their EEG recordings are partitioned into L non-overlapping segments, where interictal period are roughly of equal duration and the paired preictal period is approximately a half hour. When $L-1$ segments of the EEG data are used as the training set, the remaining segment is held out as test set. During training, the diagnosis model is trained only on 80% of the data in the training set, while the remaining 20% is used to validate for preventing overfitting. The training process stops based on the maximum iteration number and the error rate on the validation data in each training epoch. Specifically, the model either completes training after 50 iterations or stops training when the validation error rate continues to rise for four consecutive epochs. After the training of the diagnosis model is completed, it is benchmarked with the testing set following the procedure depicted in Fig. 1. After using all L segments as the testing set, the performance metrics across L independent evaluations should be averaged to obtain the cross-validation performance metrics.

When conducting the aforementioned procedures, it is important to note that two additional strategies should be employed. The first strategy entails utilizing the random oversampling technique to augment the preictal samples in the training set until the length of preictal intervals is equal to interictal intervals [41]. This is intended to mitigate the negative impact of data imbalance on the sensitivity of ResNet-50. The second strategy involves eliminating samples from the dataset that is not suitable for benchmarking. For each patient, their EEG recordings are required to comprise a minimum of 3-hour interictal intervals and two occurrences of seizure [46]. If the duration between two epileptic seizures is less than 2 hours, the latter seizure should be excluded to prevent the postictal influence of the former seizure [47].

III. RESULTS

For evaluating the epileptic seizure diagnosis, it is necessary to define beforehand the feature intervals in the prediction process, including the seizure occurrence period (SOP) and the seizure prediction horizon (SPH). The former denotes the time interval during which the seizure onset is expected to occur, while the latter refers to the period between the SOP and the epileptic warning alarm. Therefore, the SOP is located after the SPH. If the true seizure onset marker appears outside the SOP interval, the prediction is considered a failure; if it appears within the interval, it is considered successful. According to previous studies [41], [48], [49], we set the SPH to 5 minutes and the SOP to 30 minutes. To avoid repeated creation of alarms in a short time, a refractory period was implemented, which can prevent the occurrence of a second warning alarm within 30 minutes of the initial one.

In this work, three basic metrics used to evaluate the performance of diagnosis models, namely accuracy, sensitivity and false prediction rate (FPR), were adopted. They can be calculated by the following equations:

$$Accuracy = \frac{TP+TN}{TP+TN+FP+FN}, \tag{18}$$

$$Sensitivity = \frac{TP}{TP+FN}, \tag{19}$$

$$FPR = \frac{FP}{Time\ (seizure-free\ interval\ exclude\ preictal)}, \tag{20}$$

where TP and TN denote the true positive and true negative, respectively, and FP and FN denote the false positive and false negative, respectively. To avoid conflict between FPR and sensitivity, we took SF as another evaluation metric, which can be obtained using the following equation:

$$SF = \sqrt{\frac{Sensitivity^2+(1-FPR)^2}{2}}. \tag{21}$$

The higher the SF, the better is the ability of the system to classify the positive examples.

A. Baseline preprocessing methods

To validate the superiority of ASRU in improving the deep convolution network for identifying epileptic EEG, four traditional preprocessing methods were selected as baseline methods for comparison. The first and second baseline methods are the widely used bandpass filter and discrete wavelet transform (DWT), respectively. The DWT was performed with a Daubechies wavelet of order six. In the bandpass filter, 50 Hz interference was targeted with a filter between 0.5–45 Hz [50]. Irrespective of whether a bandpass filter or discrete wavelet transform method was used, the treated EEG signals lost some information. Hence, some studies directly used untreated EEG for classification without additional preprocessing, which is also the third baseline method adopted in this work. The final baseline method is a bistable SSRU, which has been previously used in cardiac signal processing [35]. To ensure a fair comparison, all modules, except for the different preprocessing methods, had the same settings.

B. Performance on the EEG of children

TABLE II
Seizure information of selected patients from the CHB-MIT dataset

Patient	Gender	Age	EE recording length (h)	Number of eligible seizures
Chb01	Female	11	34.6	6
Chb02	Male	11	27.6	3
Chb03	Female	14	28.9	6
Chb04	Male	22	23	3
Chb05	Female	7	19.1	5
Chb06	Female	1.5	30.9	7
Chb07	Female	14.5	24.6	3
Chb08	Male	3.5	11.5	5
Chb09	Female	10	54.3	4
Chb10	Male	3	29.3	7
Chb11	Female	12	32.5	3
Chb13	Female	3	18.3	6
Chb14	Female	9	9.6	6
Chb16	Female	7	10.7	5
Chb17	Female	12	16.9	3
Chb18	Female	18	28.9	4
Chb19	Female	19	26.4	3
Chb20	Female	6	21.7	5
Chb21	Female	13	19.2	4
Chb22	Female	9	11.5	3
Chb23	Female	6	21.1	5

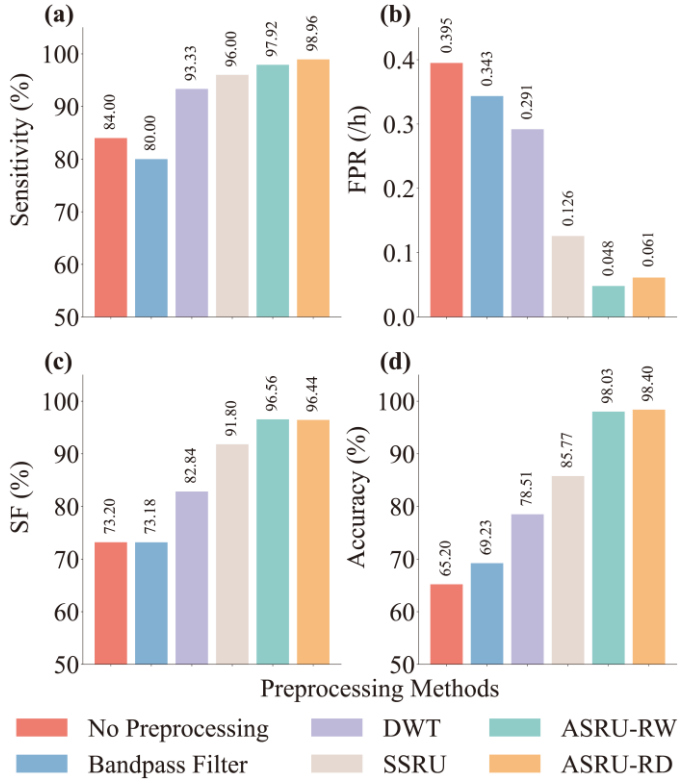

Fig. 7. (a) Precision, (b) sensitivity, (c) specificity, and (d) F1-score of epileptic EEG classification on the CHB-MIT database by the ResNet-50 with different preprocessing methods.

In this study, the proposed approach was first tested for classification on EEG datasets from children with epilepsy. The selected datasets were from the publicly available CHB-MIT database, which can be obtained from PhysioNet (https://physionet.org/content/chbmit/1.0.0/). The CHB-MIT database contains scalp EEG data from 23 children within a few days of discontinuation of antiepileptic drugs. Most of these data were collected through 23 channels with a 256 Hz sampling rate, including 844 h of continuous EEG recording. In our analysis, EEG signals recorded by all channels of the 21 qualified patients were used, and their information is presented in Table II. The selected EEG comprised 96 seizure occurrences. In this work, for the EEG signals of children, a sliding window length of 4 seconds was applied.

TABLE III
Seizure information of selected patients from the Siena dataset

Patient	Gender	Age	EE recording length (h)	Number of eligible seizures
PN01	Male	46	13.48	2
PN03	Male	54	12.53	2
PN05	Female	51	5.98	3
PN06	Male	36	12.03	5
PN09	Female	27	6.83	3
PN13	Female	34	8.65	3
PN14	Male	49	23.47	4
PN16	Female	41	5.05	2
PN17	Male	42	5.13	2

In Fig. 7, four performance metrics for epileptic EEG diagnosis on the CHB-MIT database using ResNet-50 with different preprocessing methods are presented. Compared with the no-preprocessing case, the bandpass filter-assisted ResNet-50 achieved lower FPR and higher accuracy but lower sensitivity. This can be attributed to the large amount of effective information lost during the filtering process using the bandpass filter, which also resulted in a lower SF as shown in Fig. 7(c). As compared to bandpass filters, DWT can retain more effective information while removing artifacts in the EEG [51]. Therefore, it can be observed that DWT-assisted ResNet-50 performed better in all four metrics than bandpass filter-assisted ResNet-50. Unlike bandpass filters and the DWT, the overdamped stochastic resonance unit does not lose effective EEG information. This explains why SSRU can further improve the epileptic EEG diagnosis performance of ResNet-50 compared with DWT. As ASRU enables ResNet-50 to better focus on the difference in information at different frequency intervals of EEG, the ASRU-assisted ResNet-50 can achieve a sensitivity of over 96%, an FPR below 0.06/h, an SF of over 96%, and an accuracy of over 98% while regulating both the width and depth of the potential well. Compared with ASRU-RD, the sensitivity of applying ASRU-RW was 1.04% lower, the accuracy was 0.37% lower, while the FPR was 0.013/h lower, and the SF was 0.12% higher. Thus, on the CHB-MIT database, the performance of two ASRU-assisted ResNet-50 systems is comparable but significantly superior to that of ResNet-50 assisted by other preprocessing methods.

C. Performance on the EEG of adults

To further validate the proposed method on the EEG datasets of adults with epilepsy, the publicly available Siena database was selected (https://physionet.org/content/siena-scalp-eeg/1.0.0/). The Siena database contains scalp EEG data from 14 adults within a few days of discontinuation of antiepileptic drugs. Most of these continuous EEG recordings were collected through 29 channels with a 512 Hz sampling rate. In our analysis, EEG signals recorded by all channels of the qualified 9 patients were used, and their information is

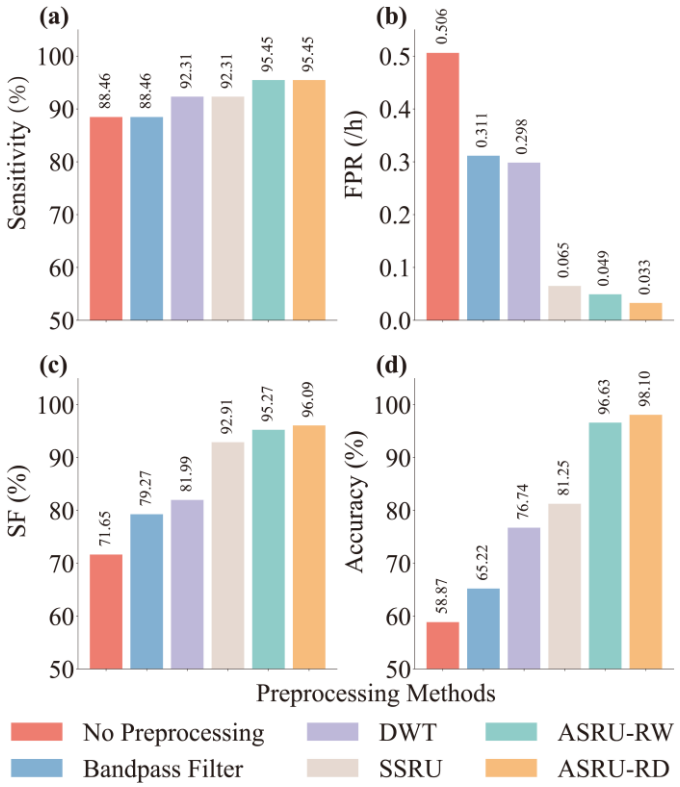

Fig. 8. (a) Precision, (b) sensitivity, (c) specificity, and (d) F1-score for epileptic EEG classification on the Siena database by the ResNet-50 with different preprocessing methods.

presented in Table III. The selected EEG comprised 22 seizure occurrence. Similar to processing the children's EEG, a sliding window length of 4 seconds was set.

In Fig. 8, four performance metrics for epileptic EEG diagnosis on the Siena database using ResNet-50 with different preprocessing methods are presented. Overall, the performance of bandpass filter-assisted ResNet-50 is superior to that of ResNet-50 without preprocessing but inferior to those of ResNet-50 assisted by other preprocessing methods. Similar to Fig. 7, the ResNet-50 assisted by DWT performs worse than the ResNet-50 assisted by SSRU. In contrast, the performance improvement achieved by applying ASRU to ResNet-50 is significantly greater than that of applying other preprocessing methods. Compared with ASRU-RW-assisted ResNet-50, the sensitivity of ASRU-RD-assisted ResNet-50 is the same, the FPR is 0.016/h lower, the SF is 0.82% higher, and the accuracy is 1.47% higher. Unlike the classification of children's EEG, the ASRU-RW lost its advantage over the ASRU-RD in FPR and SF. Therefore, on the Siena dataset, the performance of ASRU-RD-assisted ResNet-50 is better to that of ASRU-RW-assisted ResNet-50. Notably, the performance metrics of two ASRU-assisted ResNet-50 in Fig. 8 are all lesser than those in Fig. 8. This may indicate that the adult EEG signals of the Siena dataset are more difficult to classify than the child EEG signals of the CHB-MIT dataset.

D. Comparison with other learning systems with ASRU

In addition to ResNet-50, ASRU can be used as a feature extractor and denoising module for other classifiers.

TABLE IV
Performance comparison among different classifiers with different preprocessing methods on CHB-MIT datasets

Classifier	Preprocessing	Sensitivity (%)	FPR (/h)	SF (%)	Accuracy (%)
SVM	none	89.33	0.492	72.66	64.38
	SSRU	93.33	0.395	78.65	69.21
	ASRU-RW	94.67	0.137	90.58	89.07
	ASRU-RD	94.67	0.160	89.49	88.76
k-NN	none	88.00	0.469	72.66	65.39
	SSRU	92.00	0.303	81.60	70.58
	ASRU-RW	94.67	0.132	90.84	89.12
	ASRU-RD	96.00	0.126	91.80	89.55
ESN	none	92.00	0.653	69.54	59.57
	SSRU	93.33	0.366	79.77	65.86
	ASRU-RW	96.00	0.189	88.87	83.54
	ASRU-RD	96.00	0.177	89.39	83.80

TABLE V
Performance comparison among different classifiers with different preprocessing methods on Siena datasets

Classifier	Preprocessing	Sensitivity (%)	FPR (/h)	SF (%)	Accuracy (%)
SVM	none	88.46	0.545	70.35	55.22
	SSRU	92.31	0.337	80.35	62.33
	ASRU-RW	96.15	0.167	89.88	86.81
	ASRU-RD	96.15	0.156	90.48	86.28
k-NN	none	88.46	0.441	73.99	58.23
	SSRU	92.31	0.285	82.55	66.19
	ASRU-RW	96.15	0.169	89.88	90.50
	ASRU-RD	92.31	0.182	87.23	89.76
ESN	none	84.62	0.586	66.61	55.50
	SSRU	88.46	0.402	75.50	61.01
	ASRU-RW	92.31	0.285	82.55	83.09
	ASRU-RD	96.15	0.208	88.11	84.35

Experiments were conducted on both the CHB-MIT and Siena datasets with SVM, k-NN, and echo state network (ESN) classifiers separately. The first two classifiers represent conventional machine learning methods, and the ESN represents a neural network classifier without convolution operations. A linear kernel was selected for SVM. For the k-NN classifier, the number of neighbors was set to 10. The basic framework of the ESN classifier is the system used in [52]. The node number in the reservoir part of the ESN was set to 5000, and tanh nonlinearity was selected as the activation function.

The experimental results for the CHB-MIT datasets are shown in Table IV, while the results for the Siena datasets are shown in Table V. When no preprocessing method was used, the SVM, k-NN, and ESN did not perform well in classifying epileptic EEG with low SNR. For SSRU, compared with its combination with SVM and k-NN, its combination with ESN achieved the greatest performance improvement compared no preprocessing case. This is because the dynamic relaxation characteristics of the overdamped system enable it to provide a system with short-term memory capability [53], which is one of the basic abilities required for an ESN to save input information for a short time and learn its characteristics [54]. ASRU-RW and ASRU-RD significantly improved the performance of all three classifiers. This is due to the frequency domain features extracted by the ASRU while improving the EEG SNR. This also proves that ASRU can be

TABLE VI
Comparison of average processing time among different preprocessing methods

Method	Processing time (s)
Bandpass filter	0.00989
DWT	0.01009
SSRU	0.10764
ASRU	0.31952

used to enhance the performance of various classifiers when classifying epileptic EEG, in addition to the classifier based on the depth learning method.

IV. DISCUSSION

The results of the study demonstrate the superiority and versatility of the proposed ASRU as a preprocessing method for epileptic EEG classification. On the children EEG dataset, the ASRU enables ResNet-50 to obtain around 98% sensitivity. On the Siena dataset, although the sensitivity of two ASRU-assisted ResNet-50 dropped around 95%, only one seizure was identified incorrectly. These indicate This can be attributed not only to the fact that ASRU does not lose effective information in the EEG, but also to the fact that it enables the classifier to better distinguish information of abnormal neuronal activity in different frequency bands of the epileptic EEG. However, as the ASRU in the software has to rely on an iterative numerical solver such as the fourth-order Runge–Kutta algorithm, its computation speed is expected to be relatively slow compared to many traditional preprocessing methods. Table VI presents the time required to process a 4 s EEG frame intercepted by the sliding window using the different preprocessing methods. The results show that the average time required for the ASRU to process a 4 s EEG frame intercepted by the sliding window is approximately 32 times that of the average time required for the bandpass filter. At present, most classifiers used for epilepsy classification and seizure prediction tasks only require EEG signal fragments of less than 10 s; therefore, the processing time of ASRU will not exceed 1 s, and hence, this has little negative impact in clinical practice. This testing procedure was performed on a GeForce RTX 1050 notebook GPU with 6 GB memory, which is not an advanced hardware for implementation. If the hardware configuration can be improved, the computational speed of the fourth-order Runge–Kutta algorithm for solving the ASRU can be further boosted by several orders of magnitude [34].

It is worth noting that an overdamped bistable potential well can be implemented by a hardware with relatively low complexity. This indicates that ASRU can be integrated into the back-end of an EEG recording device, which is not cost-effective for some of the more sophisticated preprocessing methods [55]–[57]. As hardware-based preprocessing can avoid being subject to the von Neumann bottleneck that software-based algorithms are subject to, the ASRU implemented by hardware has the potential to achieve faster processing speeds on hardware than those listed in Table VI. Besides, traditional filters weaken the energy of the EEG signal when noise is suppressed. Hence, traditional filters implemented by hardware usually need to be accompanied by the use of low-noise amplifiers to compensate for energy loss when suppressing noise [58]. In contrast, the ASRU can amplify the EEG signal by utilizing intrinsic noise energy through the SR effect. This makes the ASRU hardware capable of realizing low-power-consumption EEG pre-processing hardware.

TABLE VII
Average computation time comparison among different classifiers

Classifier	Dataset	Computation time (s)
SVM	CHB-MIT	35.88
	Siena	8.13
k-NN	CHB-MIT	0.37
	Siena	0.30
ESN	CHB-MIT	268.74
	Siena	95.34
ResNet-50	CHB-MIT	12.46
	Siena	6.53

Table VII shows the average computation time of different classifiers assisted by ASRU to complete training and testing for one patient on two datasets. Among the classifiers, ResNet-50 exhibited a shorter computation time than that of SVM and ESN on the same dataset. Although algorithms such as ESN can speed up the operation by reducing the number of nodes in its reservoir part, it will lead to a decline in calculation accuracy. In addition, the computation time of KNN is much shorter than that of other classifiers. However, its FPR values are one order of magnitude higher than those of ResNet-50 on both datasets, indicating that KNN may lead to significant false alarm issues. Although increasing the training data may improve the FPR of KNN, it would also lead to a skyrocketing training time for KNN because of its lazy learning property [59]. Therefore, to account for both the computational speed and performance, the ASRU is more suitable for combination with the CNN classifier for epileptic EEG signals.

Over the past few decades, many different methods have been proposed for automatic diagnosis of epileptic EEG. Table VIII presents the performance comparisons of the ResNet-50 with the proposed ASRU and some recent impressive methods on the CHB-MIT dataset. Wang *et al.* [41] improved the resolution of raw EEG signals using a DWT method. In the prediction process, the deep CNN with the directed transfer function achieved an FPR of 0.08/h. Li *et al.* [46] achieved 95.50% sensitivity in epilepsy diagnosis by extracting and integrating important intrarhythm spatiotemporal features from multi-channel EEG signals using graph CNN. To preserve the spatiotemporal coupling of the epileptic cortex under different rhythms, preprocessing on EEG signals was omitted. Dissanayake *et al.* [60] preprocessed the EEG using Mel filter banks and synthesized subject-specific graphs with the obtained features using a deep graph-generating network. Thereafter, a classification-graph neural network was used to identify the status of epileptic EEG, which achieved an accuracy of 95.4%. Pandey *et al.* [61] extracted hybrid temporary features from EEG filtered using a finite impulse response (FIR) filter. Using a hybrid optimization algorithm, a deep LSTM network achieved 96.7% sensitivity to the obtained hybrid features. The methods [10] and [16] were

TABLE VIII

Performance comparison among ResNet-50 with ASRU and some existing methods on CHB-MIT datasets

Authors (Year)	Preprocessing method	Classifier	Sensitivity	FPR (/h)	SF	Accuracy
Wang *et al.* (2020) [41]	DWT	Deep CNN	90.80%	0.080	91.40%	-
Li *et al.* (2021) [46]	No processing	Graph CNN	95.50%	0.109	92.36%	-
Dissanayake *et al.* (2022) [60]	Mel filter bank	Graph Neural Network	94.47%	-	-	95.38%
Pandey et al. (2022) [61]	FIR filter	Deep LSTM	96.71%	-	-	89.91%
EPMoghaddam *et al.* (2022) [10]	DWT + Covariance matrix	SVM	93.56%	0.090	92.29%	99.1%
Singh and Lobiyal (2023) [16]	Butterworth bandpass filter	ResNet-50+LSTM	93.70%	0.056	94.08%	94.50%
Hu *et al.* (2023) [62]	DWT	Hybrid Transformer	91.70%	0	95.90%	89.00%
This work	ASRU-RW	ResNet-50	98.96%	0.048	96.56%	98.03%
This work	ASRU-RD	ResNet-50	97.92%	0.061	96.44%	98.40%

TABLE IX
Performance comparison among ResNet-50 with ASRU and some existing methods on Siena datasets

Authors (Year)	Preprocessing method	Classifier	Sensitivity	FPR (/h)	SF	Accuracy
Dissanayake *et al.* (2022) [60]	Mel filter bank	Graph neural network	96.05%	-	-	96.05%
Pandey *et al.* (2022) [61]	FIR filter	Deep LSTM	94.83%	-	-	92.59%
Fatlawi *et al.* (2022) [63]	DWT	KNN	72.59%	0.049	84.60%	93.79%
Fatlawi *et al.* (2022) [63]	DWT	Adaptive random forest	93.13%	0.033	94.93%	96.44%
Zhao *et al.* (2023) [64]	Bandpass filter	CNN+Transformer	97.40%	-	-	97.87%
This work	ASRU-RW	ResNet-50	95.45%	0.049	95.27%	96.63%
This work	ASRU-RD	ResNet-50	95.45%	0.033	96.09%	98.10%

described in the Introduction section. Notably, although the residual network in [16] connected with a LSTM was deeper than the ResNet-50 adopted in this work, their sensitivity, SF, and accuracy were only 93.70%, 94.08%, and 94.50%, respectively. This further proves the superiority of ASRU as a preprocessing module compared with traditional filter. Hu *et al.* [62] achieved 91.7% sensitivity and 0/h FPR on the CHB-MIT dataset by combining transfer learning with hybrid Transformer.

Table IX presents the performance comparisons of the ResNet-50 with proposed ASRU and some recent methods on the Siena dataset. Fatlawi *et al.* [60] used a similarity-based adaptive window to improve the unbalanced distribution of items in the EEG data stream filtered by DWT. The use of KNN as the classifier resulted in a sensitivity of only 72.59%. By replacing KNN with adaptive RF, the sensitivity was significantly improved to 93.13%. However, its F1-score was only 76%, accompanied by a significant reduction in computational efficiency. Zhao *et al.* [64] employed a CNN to extract the local features and a Transformer to extract the global features of epileptic EEG. By coupling these two kinds of features, they achieved a sensitivity of 97.40% and an accuracy of 97.87%. In addition, [60] and [61] also achieved sensitivities of 96.05% and 94.83%, respectively, in seizure detection on the Siena dataset. Whether the methods are listed in Table VIII or Table IX, compared with ResNet-50, their classifiers either have inferior performance or tend to be based on more complex fusion classifiers and deeper network structures. If only the comparison of numerical values is considered, the ASRU enables the original ResNet-50, which has a relatively simple structure, to achieve a performance exceeding that of most other approaches for diagnosing epileptic EEG signals. Nevertheless, some experimental details, such as the length of sliding window, are different in these studies. Thus, we suggest that more attention should be paid to the methods themselves rather than to the comparison with reference significance alone.

V. CONCLUSION

In this study, an ASRU-based preprocessing module was proposed for a CNN-based intelligent epilepsy EEG diagnostic system. In the ASRU, the noise in the raw EEG can be weakened by the damping effect of an overdamped potential well or can be directly transferred to the effective information of the EEG by the SR effect. In this procedure, EEG components that overlap with the noise spectrum are not removed; thus, effective information loss, which can easily arise from traditional preprocessing methods, is avoided. In addition, by paralleling three ASRUs, which differ in their asymmetric parameters, ASRU enables each input channel of the CNN to focus on the information of different frequency bands in the EEG. This effect can be analogized to the attentional mechanism or RGB decomposition in the computer vision field, which can further enhance the CNN performance. In the experimental section, the proposed ASRU combined with ResNet-50 was benchmarked on the CHB-MIT and Siena datasets for epilepsy classification. Compared with other

preprocessing methods, ASRU enabled the highest performance improvement of ResNet-50, achieving about 98% and 95% epilepsy detection sensitivity on the CHB-MIT and Siena datasets, respectively. In addition, although the ASRU was proven to work as a generalized preprocessing module in combination with other classifiers, it is more suitable for combination with CNN. Finally, the performance of ASRU-assisted ResNet-50 was compared with that of other recent methods, the results of which further prove the superiority of ASRU over other preprocessing methods.

However, the proposed ASRU module has some limitations. For example, the ASRU can cause time-domain distortion of EEG information, which is not conducive to its integration with a temporal feature-based intelligent diagnosis system. In addition, when the length of sliding window become shorter, the ASRU may destroy the information in the EEG owing to the transient dynamics at the beginning of the calculation. Hence, if the EEG fragment intercepted by the sliding window used for classification is too short, the proposed method may negatively impact the classifier. In this case, this problem can be solved by overlapping short EEG frames with a longer frame. However, this increases the computational burden. For future improvements, we recommend that three directions be considered. The first is to improve the CNN connected with ASRU. Several improved variants have been proposed based on the traditional ResNet-50 algorithm [65, 66]. Moreover, many excellent CNNs have been constructed in the field of intelligent seizure detection [16, 59]. Combining these networks with our proposed ASRU may enhance the performance. The second is to enhance the performance of ASRU. Commonly used improvement methods for nonlinear systems, such as cascading and adding feedback loops, can enhance the short-term memory capacity of the ASRU while boosting their ability to suppress noise. The third is utilizing some methods, such as Volterra model [67] and moment method [68], to estimate the noise intensity of EEG. This may aid in determining the potential parameters of ASRU without prior knowledge, thereby reducing the burden of parameter optimization. In addition to the above prospects for performance improvement, the hardware implementation of the ASRU and its integration with clinical EEG recorders are also promising.

REFERENCES

[1] A. Pitkänen, X. Ekolle Ndode-Ekane, N. Lapinlampi, and N. Puhakka, "Epilepsy biomarkers – Toward etiology and pathology specificity," *Neurobiol. Dis.*, vol. 123, pp. 42-58, *March* 2019.

[2] N. D. P. H. C. G. World Health Organization, Switzerland: World Health Organization, *Sept.* 2006. Available: https ://www.who.int/news-room/fact-sheets/detail/epilepsy

[3] A. C. Grant *et al.,* "EEG interpretation reliability and interpreter confidence: A large single-center study," *Epilepsy Behav.*, vol. 32, pp. 102-107, *March* 2014.

[4] H. Qu and J. Gotman, "Improvement in seizure detection performance by automatic adaptation to the EEG of each patient," *Electroencephalogr. Clin. Neurophysiol.*, vol. 86, no. 2, pp. 79-87, *Feb.* 1993.

[5] N. Acir, I. Oztura, M. Kuntalp, B. Baklan, and C. Guzelis, "Automatic detection of epileptiform events in EEG by a three-stage procedure based on artificial neural networks," *IEEE. Trans. Biomed. Eng.*, vol. 52, no. 1, pp. 30-40, *Jan.* 2005.

[6] O. Faust, U. R. Acharya, L. C. Min, and B. H. C. Sputh, "Automatic identification of epileptic and background EEG signals using frequency domain parameters," *Int. J. Neural. Syst.*, vol. 20, no. 2, pp. 159-176, *April* 2010.

[7] A. R. Hassan and A. Subasi, "Automatic identification of epileptic seizures from EEG signals using linear programming boosting," *Comput. Methods Programs Biomed.*, vol. 136, pp. 65-77, *Nov*. 2016.

[8] J. Gotman, "Automatic recognition of epileptic seizures in the EEG," *Electroencephalogr. Clin. Neurophysiol.*, vol. 54, no. 5, pp. 530-540, *Nov.* 1982.

[9] J. R. Williamson, D. W. Bliss, D. W. Browne, and J. T. Narayanan, "Seizure prediction using EEG spatiotemporal correlation structure," *Epilepsy Behav.*, vol. 25, no. 2, pp. 230-238, *Oct.* 2012.

[10] D. EPMoghaddam, S. A. Sheth, Z. Haneef, J. Gavvala, and B. Aazhang, "Epileptic seizure prediction using spectral width of the covariance matrix," *J. Neural Eng.*, vol. 19, no. 2, *April* 2022, Art. no. 026029.

[11] M. Mursalin, Y. Zhang, Y. Chen, and N. V. Chawla, "Automated epileptic seizure detection using improved correlation-based feature selection with random forest classifier," *Neurocomputing*, vol. 241, pp. 204-214, *June* 2017.

[12] F. Celesti, A. Celesti, J. Wan, and M. Villari, "Why Deep Learning Is Changing the Way to Approach NGS Data Processing: A Review," *IEEE Rev. Biomed. Eng.,* vol. 11, pp. 68-76, *April* 2018.

[13] M. P. Hosseini, A. Hosseini, and K. Ahi, "A Review on Machine Learning for EEG Signal Processing in Bioengineering," *IEEE Rev. Biomed. Eng.,* vol. 14, pp. 204-218, *Jan.* 2020.

[14] O. M. A. Ali, S. W. Kareem, and A. S. Mohammed, "Evaluation of Electrocardiogram Signals Classification Using CNN, SVM, and LSTM Algorithm: A review," in 2022 *8th International Engineering Conference on Sustainable Technology and Development (IEC)*, 2022, pp. 185-191.

[15] U. R. Acharya, S. L. Oh, Y. Hagiwara, J. H. Tan, and H. Adeli, "Deep convolutional neural network for the automated detection and diagnosis of seizure using EEG signals," *Comput. Biol. Med.*, vol. 100, pp. 270-278, *Sept.* 2018.

[16] Y.P. Singh and D.K. Lobiyal, " Automatic prediction of epileptic seizure using hybrid deep ResNet-LSTM model," *AI Commun.,* vol. 36, no. 1, pp. 57-72, *Feb.* 2023.

[17] Y. Zhang, Y. Guo, P. Yang, W. Chen, and B. Lo, "Epilepsy Seizure Prediction on EEG Using Common Spatial Pattern and Convolutional Neural Network," *IEEE J. Biomed. Health. Inform.*, vol. 24, no. 2, pp. 465-474, *Feb.* 2020.

[18] N. D. Truong *et al.,* "Convolutional neural networks for seizure prediction using intracranial and scalp electroencephalogram," *Neural Netw.*, vol. 105, pp. 104-111, *Sept.* 2018.

[19] R. Romo Vázquez, H. Vélez-Pérez, R. Ranta, V. Louis Dorr, D. Maquin, and L. Maillard, "Blind source separation, wavelet denoising and discriminant analysis for EEG artefacts and noise cancelling," *Biomed. Signal Process. Control,* vol. 7, no. 4, pp. 389-400, *July* 2012.

[20] J. Rasekhi, M. R. K. Mollaei, M. Bandarabadi, C. A. Teixeira, and A. Dourado, "Preprocessing effects of 22 linear univariate features on the performance of seizure prediction methods," *J. Neurosci. Methods*, vol. 217, no. 1, pp. 9-16, *July* 2013.

[21] Y. Gao, B. Gao, Q. Chen, J. Liu, and Y. Zhang, "Deep Convolutional Neural Network-Based Epileptic Electroencephalogram (EEG) Signal Classification," *Front. Neurol.,* vol. 11, *May* 2020, Art. no. 375.

[22] S. M. Usman, M. Usman, and S. Fong, "Epileptic Seizures Prediction Using Machine Learning Methods," *Comput. Math. Methods Med.*, vol. 2017, *Dec.* 2017. Art. no. 9074759.

[23] X. Wang, I. Ounis, and C. Macdonald, "Negative confidence-aware weakly supervised binary classification for effective review helpfulness classification," in *Proceedings of the 29th ACM International Conference on Information & Knowledge Management*, 2020, pp. 1565-1574.

[24] B. McNamara and K. Wiesenfeld, "Theory of stochastic resonance," *Phys. Rev. A*, vol. 39, no. 9, p. 4854, *May* 1989.

[25] Z. Wang, J. Yang, Y. Guo, T. Gong, and Z. Shan, "Positive role of bifurcation on stochastic resonance and its application in fault diagnosis under time-varying rotational speed," *J. Sound Vib.*, vol. 537, *Oct*. 2022. Art. no. 117210.

[26] M. Li, P. Shi, W. Zhang, and D. Han, "A novel underdamped continuous unsaturation bistable stochastic resonance method and its application," *Chaos, Solitons and Fractals,* vol. 151, *Oct*. 2021. Art. no.

111228.
[27] Z. Qiao and X. Shu, "Coupled neurons with multi-objective optimization benefit incipient fault identification of machinery," *Chaos, Solitons and Fractals*, vol. 145, *April* 2021. Art. no. 110813.
[28] Y. Fu, Y. Kang, and G. Chen, "Stochastic Resonance Based Visual Perception Using Spiking Neural Networks," *Front. Comput. Neurosci.,* vol. 14, p. 11, *May* 2020, Art. no. 24.
[29] S. Bai, F. Duan, F. Chapeau-Blondeau, and D. Abbott, "Generalization of stochastic-resonance-based threshold networks with Tikhonov regularization," *Phys. Rev. E,* vol. 106, no. 1, *July* 2022. Art. no. L012101.
[30] L. Duan, Y. Ren, and F. Duan, "Adaptive stochastic resonance based convolutional neural network for image classification," *Chaos, Solitons & Fractals*, vol. 162, *Sept*. 2022. Art. no. 112429.
[31] D. F. Russell, L. A. Wilkens, and F. Moss, "Use of behavioural stochastic resonance by paddle fish for feeding," *Nature*, vol. 402, no. 6759, pp. 291-294, *Nov*. 1999.
[32] R. K. Christensen, H. Lindén, M. Nakamura, and T. R. Barkat, "White Noise Background Improves Tone Discrimination by Suppressing Cortical Tuning Curves," *Cell Rep.*, vol. 29, no. 7, pp. 2041-2053.e4, *Nov.* 2019.
[33] M. Singh, A. Verma, and N. Sharma, "Optimized multistable stochastic resonance for the enhancement of pituitary microadenoma in MRI," *IEEE J. Biomed. Health. Inform.,* vol. 22, no. 3, pp. 862-873, *June* 2017.
[34] C. B. Güngör, P. P. Mercier, and H. Töreyin, "A Stochastic Resonance Electrocardiogram Enhancement Algorithm for Robust QRS Detection," *IEEE J. Biomed. Health. Inform.,* vol. 26, no. 8, pp. 3743-3754, *May* 2022.
[35] Z. Liao, S. Jin, A. Kuwahata, M. Sekino, and H. Tabata, "Coherent detection stochastic resonance assisted biomagnetometer for measuring magnetocardiography at room temperature," *Appl. Phys. Express*, vol. 14, no. 9, *Aug.* 2021, Art. no. 097001.
[36] L. J. Rogers, P. Zucca, and G. Vallortigara, "Advantages of having a lateralized brain," *Proc. Royal Soc. B*, vol. 271, no. suppl_6, pp. S420-S422, *Dec*. 2004.
[37] K. He, X. Zhang, S. Ren, and J. Sun, "Deep residual learning for image recognition," in *Proceedings of the IEEE conference on computer vision and pattern recognition*, 2016, pp. 770-778.
[38] N. Carion, F. Massa, G. Synnaeve, N. Usunier, A. Kirillov, and S. Zagoruyko, "End-to-end object detection with transformers," in *ECCV*, 2020, pp. 213-229.
[39] S. Sareen, S. K. Sood, and S. K. Gupta, "An Automatic Prediction of Epileptic Seizures Using Cloud Computing and Wireless Sensor Networks," *J. Med. Syst.*, vol. 40, no. 11, p. 226, *Sept.* 2016.
[40] P. Thodoroff, J. Pineau, and A. Lim, "Learning robust features using deep learning for automatic seizure detection," in *Machine learning for healthcare conference*, 2016, pp. 178-190.
[41] G. Wang *et al.*, "Seizure Prediction Using Directed Transfer Function and Convolution Neural Network on Intracranial EEG," *IEEE Trans. Neural Syst. Rehabilitation Eng.*, vol. 28, no. 12, pp. 2711-2720, *Dec*. 2020.
[42] L. Chen and J.-Q. Sun, "The closed-form solution of the reduced Fokker–Planck–Kolmogorov equation for nonlinear systems," *Commun. Nonlinear Sci. Numer. Simul.*, vol. 41, pp. 1-10, *Dec.* 2016.
[43] M. A. Fuentes, R. Toral, and H. S. Wio, "Enhancement of stochastic resonance: the role of non Gaussian noises," *Physica. A*, vol. 295, no. 1, pp. 114-122, *June* 2001.
[44] Z. Liao, Z. Wang, H. Yamahara, and H. Tabata, "Low-power-consumption physical reservoir computing model based on overdamped bistable stochastic resonance system," *Neurocomputing*, vol. 468, pp. 137-147, *Oct*. 2021.
[45] T. Akiba, S. Sano, T. Yanase, T. Ohta, and M. Koyama, "Optuna: A next-generation hyperparameter optimization framework," in *Proceedings of the 25th ACM SIGKDD international conference on knowledge discovery & data mining*, 2019, pp. 2623-2631.
[46] Y. Li, Y. Liu, Y. Guo, X. Liao, B. Hu, and T. Yu, "Spatio-temporal-spectral hierarchical graph convolutional network with semisupervised active learning for patient-specific seizure prediction," *IEEE Trans. Cybern.*, vol. 52, no. 11, pp. 12189 - 12204, May 2021.
[47] D. E. Snyder, J. Echauz, D. B. Grimes, and B. Litt, "The statistics of a practical seizure warning system," *J. Neural Eng.*, vol. 5, no. 4, pp. 392–401, *Sep*. 2008.
[48] H. Khan, L. Marcuse, M. Fields, K. Swann, and B. Yener, ''Focal onset seizure prediction using convolutional networks,'' *IEEE Trans. Biomed. Eng.*, vol. 65, no. 9, pp. 2109–2118, *Sep*. 2017.
[49] D. Liang, A. Liu, L. Wu, C. Li, R. Qian, R. K. Ward, and X. Chen, "Semisupervised seizure prediction in scalp EEG using consistency regularization," *J. Healthc. Eng.*, vol. 2022, *Jan*. 2022. Art. no. 1573076.
[50] D. P. Dash and M. H. Kolekar, "Hidden Markov model based epileptic seizure detection using tunable Q wavelet transform," *J. Biomed. Res.*, vol. 34, no. 3, p. 170, *May* 2020.
[51] M. J. Ferdous, M. S. Ali, M. E. Hamid, and M. K. I. Molla, "A comparison of butterworth bandpass filter and discrete wavelet transform filter for the suppression of ocular artifact from EEG signal," *Int. J. Res. Eng. Technol. Sci.*, vol. 1, no. 4, *June* 2016.
[52] L. Sun, B. Jin, H. Yang, J. Tong, C. Liu, and H. Xiong, "Unsupervised EEG feature extraction based on echo state network," *Inf. Sci.*, vol. 475, pp. 1-17, *Feb.* 2019.
[53] Z. Liao, Z. Wang, H. Yamahara, and H. Tabata, "Echo state network activation function based on bistable stochastic resonance," *Chaos Solitons Fractals*, vol. 153, *Dec*. 2021, Art. no. 111503.
[54] H. Jaeger, "Short term memory in echo state networks," *GMD-Forschungszentrum Informationstechnik*, 2001.
[55] D. Hu, J. Cao, X. Lai, J. Liu, S. Wang, and Y. Ding, "Epileptic Signal Classification Based on Synthetic Minority Oversampling and Blending Algorithm," *IEEE Trans. Cogn. Develop. Syst.*, vol. 13, no. 2, pp. 368-382, *June* 2021.
[56] S. K. Khare, V. Bajaj, and U. R. Acharya, "SPWVD-CNN for Automated Detection of Schizophrenia Patients Using EEG Signals," *IEEE Trans. Instrum. Meas.*, vol. 70, pp. 1-9, *April* 2021.
[57] C. Lei *et al.,* "Epileptic Seizure Detection in EEG Signals Using Discriminative Stein Kernel-Based Sparse Representation," *IEEE Trans. Instrum. Meas.*, vol. 71, pp. 1-15, *Dec*. 2022.
[58] S. J. Johnstone, R. Blackman, and J. M. Bruggemann, "EEG From a Single-Channel Dry-Sensor Recording Device," *Clin. EEG Neurosci.*, vol. 43, no. 2, pp. 112-120, *April* 2012.
[59] M. Manjusha and R. Harikumar, "Performance analysis of KNN classifier and k-means clustering for robust classification of epilepsy from EEG signals," in *Proc. IEEE Int. Conf. Wireless Commun., Signal Process. Netw.*, 2016, pp. 2412–2416.
[60] T. Dissanayake, T. Fernando, S. Denman, S. Sridharan, and C. Fookes, "Geometric Deep Learning for Subject Independent Epileptic Seizure Prediction Using Scalp EEG Signals," *IEEE J. Biomed. Health. Inform.,* vol. 26, no. 2, pp. 527-538, *Feb*. 2022.
[61] A. Pandey, S. K. Singh, S. S. Udmale, and K. K. Shukla, "Epileptic Seizure Classification Using Battle Royale Search and Rescue Optimization-Based Deep LSTM," *IEEE J. Biomed. Health. Inform.*, vol. 26, no. 11, pp. 5494-5505, *Nov*. 2022.
[62] S. Hu *et al.*, "Exploring the Applicability of Transfer Learning and Feature Engineering in Epilepsy Prediction Using Hybrid Transformer Model," *IEEE Trans. Neural Syst. Rehabilitation Eng.*, vol. 31, pp. 1321-1332, *Feb*. 2023.
[63] H. K. Fatlawi and A. Kiss, "Similarity-Based Adaptive Window for Improving Classification of Epileptic Seizures with Imbalance EEG Data Stream," *Entropy*, vol. 24, no. 11, p. 1641, *Nov*. 2022.
[64] Y. Zhao *et al.*, "Interactive local and global feature coupling for EEG-based epileptic seizure detection," *Biomed. Signal Process. Control.*, vol. 81, *Mar*. 2023, Art. no. 104441.
[65] B. Li and Y. He, "An Improved ResNet Based on the Adjustable Shortcut Connections," *IEEE Access*, vol. 6, pp. 18967-18974, *Mar*. 2018.
[66] Z. Lu *et al*., "The classification of gliomas based on a Pyramid dilated convolution resnet model," *Pattern Recognit. Lett.,* vol. 133, pp. 173-179, *May* 2020.
[67] M. Hassani and M. Karami, "Noise estimation in electroencephalogram signal by using volterra series coefficients," *J. Medical Signals Sens.*, vol. 5, pp. 192–200, *July* 2015.
[68] Y. Fu, Y. Kang, and R. Liu, "Novel bearing fault diagnosis algorithm based on the method of moments for stochastic resonant systems," *IEEE Trans. Instrum. Meas.*, vol. 70, pp. 1–10, *Aug*. 2020, Art. no. 6500610.